Field induced topological Hall effect and double fan spin structure with *c*-axis component in metallic kagome antiferromagnetic YMn_6Sn_6

Qi Wang[1,#], Kelly J. Neubauer[2,#], Chunruo Duan[2,#], Qiangwei Yin[1], Satoru Fujitsu[3], Hideo Hosono[3,4], Feng Ye[5], Rui Zhang[2], Songxue Chi[5], Kathryn Krycka[6], Hechang Lei[1,*], and Pengcheng Dai[2,*]

[1] *Department of Physics and Beijing Key Laboratory of Opto-electronic Functional Materials & Micro-nano Devices, Renmin University of China, Beijing 100872, China*

[2] *Department of Physics and Astronomy, Rice University, Houston, Texas 77005, USA*

[3] *Materials Research Center for Element Strategy, Tokyo Institute of Technology, Yokohama 226-8503, Japan*

[4] *Laboratory for Materials and Structures, Tokyo Institute of Technology, Yokohama 226-8503, Japan*

[5] *Neutron Scattering Division, Oak Ridge National Laboratory, Oak Ridge, Tennessee 37831, USA*

[6] *NIST Center for Neutron Research, National Institute of Standards and Technology, Gaithersburg, MD 20899, USA*

[#] These authors contributed to this work equally.

Corresponding authors: hlei@ruc.edu.cn, pdai@rice.edu

Supplementary Material

Supplemental Note

SN1: Single crystal growth

YMn_6Sn_6 single crystals were grown by the Sn flux method. The starting materials Y lumps (purity 99.99 %), Mn granules (purity 99.9 %) and Sn grains (purity 99.99 %) were mixed together in a molar ratio of Y : Mn : Sn = 1 : 6 : 30 and put into an alumina crucible. Then, the crucible was sealed in a quartz ampoule under partial argon atmosphere. The sealed quartz ampoule was heated up to 1273 K and kept there for 24 h to ensure the homogeneity of melt. After that the ampoule was cooled down slowly to 873 K in 80 h. At this temperature, the ampoule was taken out from the furnace and decanted with a centrifuge to extract YMn_6Sn_6 single crystals from the Sn flux.

SN2: Magnetization and Transport measurements

Magnetization and electrical transport measurements were performed in Quantum Design PPMS-14 T. Both longitudinal and Hall electrical resistivity were measured simultaneously in a standard five-probe configuration. For measuring ϱ_{xx} ($I \parallel V \parallel [100]$, $B \parallel [001]$) and ϱ_{yx} ($I \parallel [100]$, $V \parallel [120]$, $B \parallel [001]$), the crystal with size about $2.0 \times 1.5 \times 0.2$ mm^3 was used and the Pt wires are stick on the sample directly using Ag epoxy. For measuring ϱ_{zz} ($I \parallel V \parallel [001]$, $B \parallel [100]$) and ϱ_{yz} ($I \parallel [001]$, $V \parallel [120]$, $B \parallel [100]$), the samples were fabricated into rectangular shape using the focus ion beam (FIB) technique by using JEOL JEM-9320FIB (Fig. S1). The W contacts were deposited between the sample and Au pads and then the Pt wires were connected on the Au pads using Ag paste. In order to effectively get rid of the longitudinal resistivity contribution due to voltage probe misalignment, we measured the Hall resistivity at positive and negative fields. The total Hall resistivity was determined by $\varrho_H(B) = [\varrho_H(+B) - \varrho_H(-B)]/2$. Correspondingly, the longitudinal resistivity was obtained by $\varrho(B) = [\varrho(+B) + \varrho(-B)]/2$.

SN3: Neutron diffraction Measurements

The aim of the following neutron diffraction measurements was to connect the observed THE in YMn_6Sn_6 to its unknown magnetic structure. In several materials including MnSi [1] and Gd_2PdSi_3 [2], a skyrmion phase was observed that coincides with the measurement of the THE.

Skyrmions stabilized by Dzyaloshinskii-Moriya interaction (DMI) typically range from 1–100 nm in size varying with material parameters, applied magnetic field, and temperature [2]. Considering this possibility of a skyrmion lattice in YMn_6Sn_6, small angle neutron scattering (SANS) was performed at the NG7 SANS instruments at the NIST Center for Neutron Research (NCNR). A 9 T horizontal field magnet was used with two orientations $B \parallel [100]$ and $B \parallel [001]$ through a temperature range of 5 to 300 K. Two configurations with sample to detector distances of 15.3 m and 2 m were used to span a total range of q from ~ 0.002 to 0.125 $Å^{-1}$. No skyrmion lattice signatures were observed under any temperature or field orientation throughout this q range. The absence of skyrmions is shown at 240 K, 3.5 T in the 15.3 m detector configuration in Fig. S5(a) and the 2 m detector configuration in Fig. S5(b). Instead, we determine the non-collinear spin texture of YMn_6Sn_6 with wide angle neutron measurements.

Wide angle single-crystal neutron diffraction measurements were performed on the CORELLI elastic diffuse scattering spectrometer at the Spallation Neutron Source (SNS), Oak Ridge Nation Laboratory (ORNL) [3] and at the HB-3 thermal neutron triple-axis spectrometer at the High Flux Isotope Reactor (HFIR), ORNL. At CORELLI, a single crystalline YMn_6Sn_6 sample was mounted to an Al rod and oriented in the $[H, 0, L]$ and $[H, K, 0]$ scattering planes. The mounted samples are shown for the field in-plane along $[1, 0, 0]$ orientation in Fig. S6(a) and field out-of-plane along [0, 0, 1] orientation in Fig. S6(b). A 5 T vertical field superconducting magnet with a top loading closed cycled refrigerator was used and covered temperatures between 2 and 240 K and magnetic fields up to its maximum of 5 T. Data was collected with a white incident beam while rotating the sample through a 360° range with a 1.5° step size for 3 minutes at each angle. In Fig. S7(a), the zero-field 2 K data for sample 1 is shown and the incommensurate satellite peaks corresponding to wavevector $\delta = 0.261(8)$ are observed. In Fig. S7(b), a 5 T magnetic field has been applied to sample 1. Cuts along $[H, 0, L]$ for $H = 1$ are seen in Fig. S8. A peak is observed at $\delta = 0.2653(19)$ and 2δ. Since δ is close to 1/4, the 2δ peaks overlap near $(1, 0, 0.5)$ as shown in the inset. Measurements were repeated with a second single crystal sample. The results with sample 2 are consistent with sample 1 except for a slight change in incommensurability. This is shown in Fig. S7(c) where the zero-field 2 K data has incommensurate peaks corresponding to $\delta = 0.2653(19)$ and in Fig. S7(d) where the application of 5 T peaks results in peaks at δ and 2δ with $\delta = 0.2799(19)$.

Additional measurements were done to closely study the evolution of the incommensurate peak with applied field. With sample 1 in a fixed orientation of 16.5° and temperature of 2 K, field was swept in 0.25 T increments with 5 minutes per increment between 0 and 5 T. This was also done at 240 K as shown in Fig. S9. The same [H, 0, L] reciprocal space maps were obtained at 240 K for 0 T [Fig. S9(a)], 3 T [Fig. S9(b)], and 5 T [Fig. S9(c)]. At 0 T, a peak is observed at δ = 0.2830(19). At 3 T, a peak is observed at δ = 0.3352(19). Since this peak is ~ 1/3, the 2δ overlaps with δ and does not show up as a distinct peak as it does at 2 K. For field perpendicular to the plane and measuring in the [H, K, 0] scattering plane, intensity is only observed at the Bragg peaks at 2 K, 0 T [Fig. S10(a)], 2 K, 5 T [Fig. S10(b)], and 240 K, 5 T [Fig. S10(c)].

Neutron diffraction measurements were also performed on HB-3 at ORNL. In Fig. S6(c), the single crystal mounted in the [H, 0, L] scattering plane at HB-3 is shown. An 8 T vertical magnetic field with a top loading closed cycled refrigerator was used to cover temperatures between 20 and 240 K and magnetic fields up to its maximum 8 T. Measurements were taken with incident and out-going neutron energies of $E_i = E_f$ =14.7 meV. The measurements taken below 5 T are consistent with our results from CORELLI. Above 5 T, we observe a new peak at (0, 0, 1/2) that has a maximum intensity at 6.5 T as shown in Fig. S11(a). The temperature dependence of this peak was also measured [Fig. S11(b)]. This indicates that a new phase exists in the high field and low temperature regime, but further measurements will be required to fully characterize it. This regime is shown in the main text in Fig. 5(a) and is denoted by "?" state.

SN4: Neutron Data Refinement

The Mantid package was used for data reduction [4]. For each reciprocal space map, the peak intensities for peaks in the [H, 0, L] scattering plane were found by integrating along the [H, 0, 0] and [0, K, 0] directions with ΔH = 0.1 and ΔK = 0.1 resulting in cuts along [0, 0, L]. A cut of [1, 0, L] at 2 K with fields of 0 T and 5 T is shown in Fig. S8 and [0,0,L] and [2, 0, L] is shown in the main text. Each peak along the [0, 0, L] cut was fit to a Gaussian to determine its intensity and position of the peak or wavevector δ. The Gaussian fit for several peaks has been included in Figs. S12(a) - (d) showing their response to magnetic field. In all cases, we find that the magnetic Bragg peaks are instrumental resolution limited, indicating a

homogeneous field-induced structure. Incommensurability varies slightly by sample and δ increases with increasing temperature. Using the determined peak intensities at each Bragg peak in zero-field, the FULLPROF software was used to refine the nuclear structure of YMn_6Sn_6 [5]. The result of this refinement is seen in Fig. S13(a). The zero-field magnetic refinements of CORELLI neutron diffraction data were carried out with the Jana2006 software for the helical antiferromagnetic (H-AFM) structure [6]. The non-centrosymmetric super-space group $P6.1'(00g)$-hs was used for the refinement of the incommensurate peaks in zero-field. The fitting was done at both 2 K and 240 K with an increased rotating angle δd between layers at 240 K. The 2 K results are included in Fig. S13(b).

SN5: Least Square Fitting on the Incommensurate Peak Intensities with Magnetic Field

As demonstrated in the main text, the diffraction pattern of YMn_6Sn_6 under in-plane magnetic field developed a series of incommensurate peaks with non-zero H indices, and therefore cannot be reproduced by the refined magnetic structure under zero magnetic field. Since magnetic neutron scattering function is proportional to the spin component that is perpendicular to the momentum transfer $\boldsymbol{Q}$, this strongly indicates that a non-zero c-axis component exists in the magnetic structure under field. A spin structure model with fan-like configuration in both ab-plane and c-axis has been considered. The model has three parameters, the in-plane spreading angle ϕ_{ab}, the c-axis spreading angle ϕ_c, and the phase difference φ between these two components. The magnetic contribution to the elastic channel of the neutron scattering function $S(\boldsymbol{Q})$ can be calculate on a simulated lattice with 200 layers. The spins from each layer are considered to be collinear. To determine these parameters based on the observed incommensurate intensities, least square fittings on the calculated $S(\boldsymbol{Q})$ versus observed $S(\boldsymbol{Q})$ have been performed with a large set of parameter combinations on two data sets.

For the datasets collected at 2 K, 5 T, the incommensurability is 0.26, very close to the commensurate wave vector of 1/4. As a result, secondary satellite peaks from adjacent Bragg positions overlap at half-integer L positions. This provides extra constrain over the fitting parameters. First, the spreading angle ϕ_{ab} was determined by fitting a dataset with 16 incommensurate peaks along the (0, 0, L) cut, as shown in Fig S14(a). This is because the spreading of spins along the c-axis has little influences on the $H = 0$ reflections. The optimal

fitting result was obtained with $\phi_{ab} = 0.24\pi$. Then a 2D iteration of the rest two parameters, ϕ_c and φ was performed on the whole dataset of 40 reflections including $(0, 0, L)$, $(1, 0, L)$ and $(2, 0, L)$ cuts. The map of the inverse χ^2 is plotted in Fig S14(b). The optimal parameter combination is $\phi_c = 0.265\pi$, $\varphi = 0.656\pi$. The overall χ^2 is 5.50 and the quality of the optimal fitting is shown in Fig. S14(c).

For the data set collected at 240 K, 3 T, the incommensurability is 0.31. The incommensurate peak intensities of this data set are 3 to 5 times weaker than the previous dataset, and no secondary satellite peaks can be identified. Therefore, the constrain from this dataset of 33 reflections from the $(0, 0, L)$, $(1, 0, L)$ and $(2, 0, L)$ cuts on the fitting parameters is not enough to determine an optimal combination. Instead, the overall χ^2 can reach the optimal value of 1.53 if ϕ_{ab} and ϕ_c follows the curve shown in Fig S15(a) and $\varphi = 0.65\pi$. To further determine the parameter ϕ_{ab} and ϕ_c, the total magnetization with different choices of ϕ_{ab} and φ was calculated, assuming ϕ_{ab} and ϕ_c follow the curve in Fig S15(a). From magnetization measurement we know the total moment at 3 T at 240 K is in the range of 0.3 to 0.35, as shown with the red curves in Fig S15(b). Then the intersection of the $\varphi = 108$ dashed line and the red curves gives the optimal parameter set to be $\phi_{ab} = 0.455\pi$, $\phi_c = 0.38\pi$, $\varphi = 0.60\pi$. The overall χ^2 is 1.53 and the quality of the optimal fitting is shown in Fig. S15(c).

References

[1] S. Mühlbauer, B. Binz, F. Jonietz, C. Pfleiderer, A. Rosch, A. Neubauer, R. Georgii, and P. Böni, *Science* **323**, 915-919 (2009).

[2] M. Hirschberger, T. Nakajima, S. Gao, L. Peng, A. Kikkawa, T. Kurumaji, M. Kriener, Y. Yamasaki, H. Sagayama, H. Nakao, K. Ohishi, K. Kakurai, Y. Taguchi, X. Yu, T.-h. Arima, and Y. Tokura, *Nature Commun*. **10**, 5831 (2019).

[3] F. Ye, Y. Liu, R. Whitfield, R. Osborn, and S. Rosenkranz, *J. Appl. Cryst*. **51**, 315-322 (2018).

[4] J. W. Taylor, O. Arnold, J. Bilheaux, A. Buts, S. I. Campbell, M. Doucet, N. Draper, R. Fowler, M. Gigg, V. E. Lynch, A. J. Markvardsen, K. Palmen, P. A. Parker, P. F. Peterson, S. X. Ren, M. A. Reuter, A. T. Savici, R. J. K. Taylor, R. N. Tolchenov, R. Whitley, and W. Zhou, J. Zikovsky. (APS March Meeting 2012), vol. abstract id. W26.010.

[5] T. Roisnel, J. Rodriguez-Carvajal, *Mater. Sci. Forum* **378-381**, 118-123 (2001).

[6] P. Václav, D. Michal, and P. Lukáš, *Z. Kristall. – Cryst. Mater.* **229**, 345-352 (2014).

Supplementary Figures

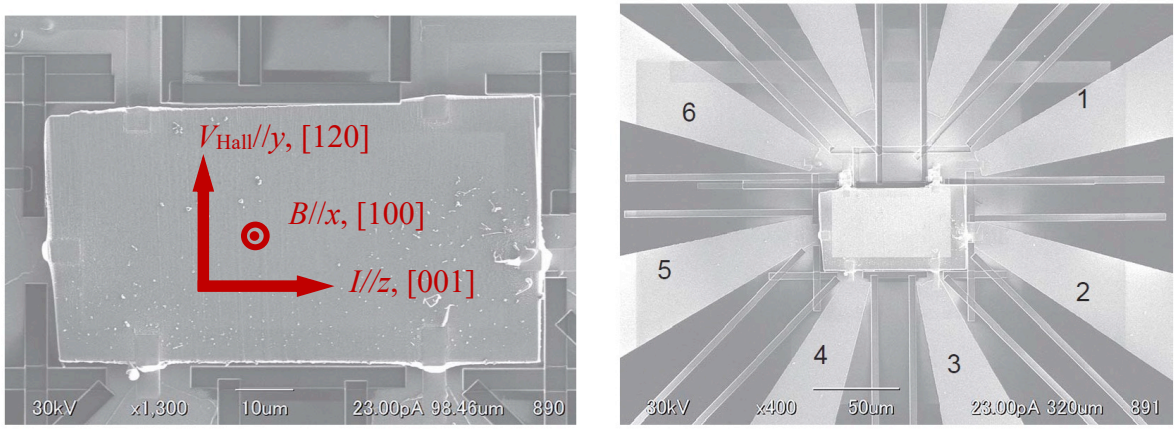

Figure S1. The five-probe configuration of ρ_{yz} and ρ_{zz} measurement for the sample fabricated by the focus ion beam (FIB) technique. The contacts 2 and 5 are for I^+ and I^-, the contacts 1 and 6 are for V^+ and V^- of ρ_{zz} and the contact 4 and 6 are for V_{Hall}^+ and V_{Hall}^- of ρ_{yz}.

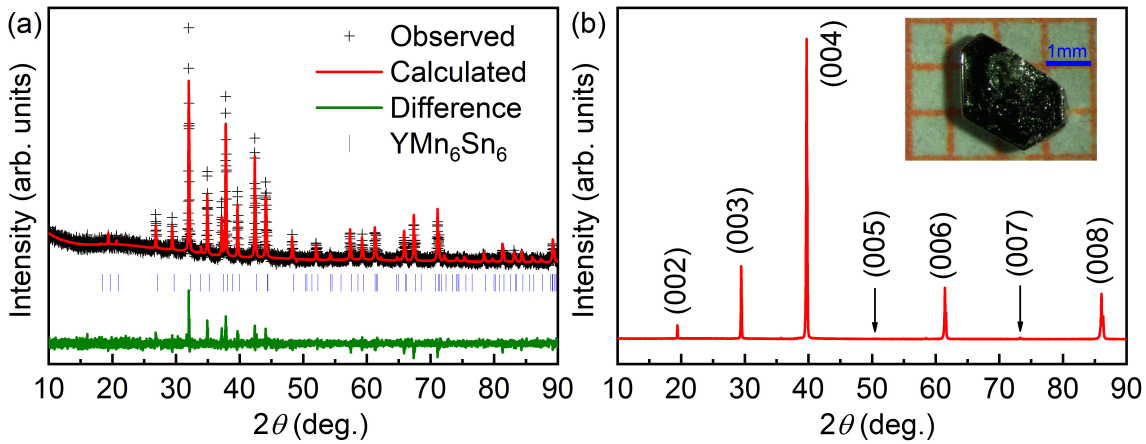

Figure S2. (a) Powder XRD pattern and the Rietveld refinement of ground YMn_6Sn_6 single crystals. The fitted lattice parameters are $a = b = 5.5362(2)$ Å and $c = 9.0146(3)$ Å. (b) XRD pattern of a YMn_6Sn_6 single crystal. All of peaks can be indexed by the indices of (00*l*) lattice planes. It reveals that the crystal surface is normal to the *c* axis with the plate-shaped surface parallel to the *ab* plane. Inset: photo of typical YMn_6Sn_6 single crystals on a 1 mm grid paper.

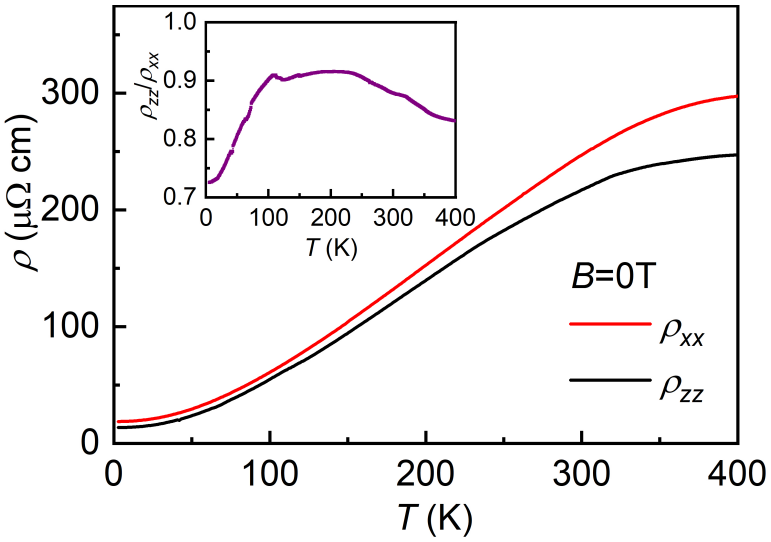

Figure S3. Zero-field longitudinal resistivity $\rho_{xx}(T)$ and $\rho_{zz}(T)$ as a function of T. Inset: temperature dependence of the ratio $\rho_{zz}(T)/\rho_{xx}(T)$. Zero-field longitudinal resistivity $\rho_{xx}(T)$ and $\rho_{zz}(T)$ display metallic behaviours between 3 and 400 K. There is an increase of slope of resistivity curves below T_N, corresponding to the suppression of spin disorder scattering. The ratio of $\rho_{zz}(T)/\ \rho_{xx}(T)$ is about 0.7 - 0.9, i.e., the even larger *c*-axial conductivity than that in the *ab* plane, suggesting that YMn_6Sn_6 should be regarded as a three-dimensional (3D) rather than two-dimensional (2D) metallic antiferromagnet.

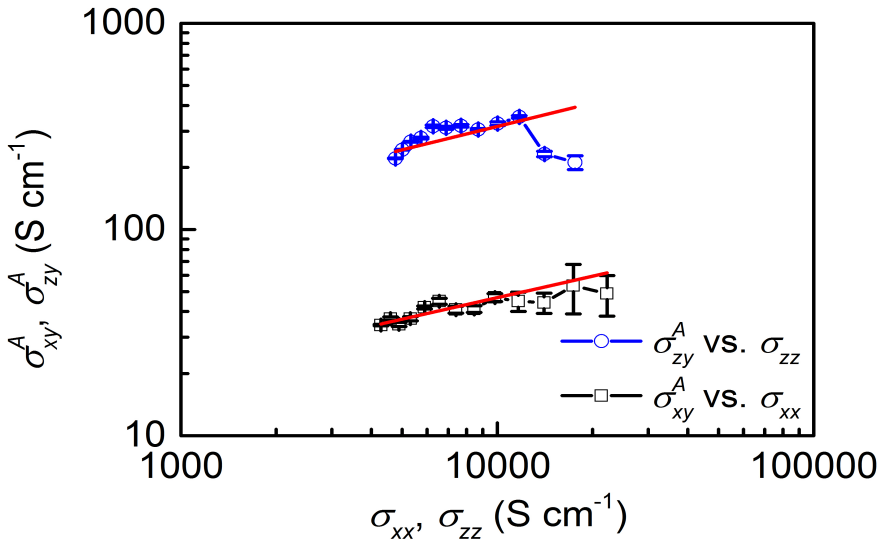

Figure S4. Relationship between the anomalous Hall conductivity $\sigma_H{}^A$ (σ_{xy} or σ_{zy}) and the longitudinal conductivity σ (σ_{xx} or σ_{zz}). The red solid lines represent the fits using the formula $\sigma_H{}^A \propto \sigma^\alpha$. The fitted α equals 0.35(6) and 0.4(1) for $\sigma_{xy}{}^A$ and $\sigma_{zy}{}^A$, respectively. It confirms the AHE at high-field region is intrinsic.

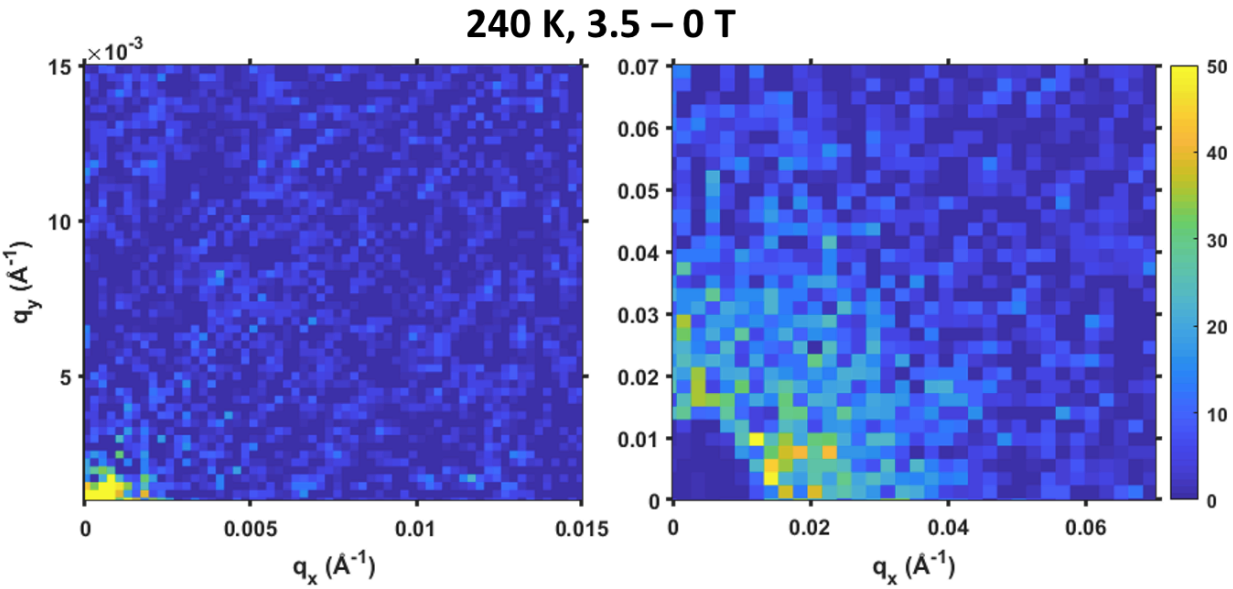

Figure S5. Raw data of the SANS pattern of YMn_6Sn_6 at 240 K, 3.5 - 0 T at two different detector configurations, (a) 15.3 m and (b) 2 m, with different q ranges. Throughout these *q* ranges where skyrmions have been observed in other materials, YMn_6Sn_6 does not exhibit any skyrmion lattice signatures.

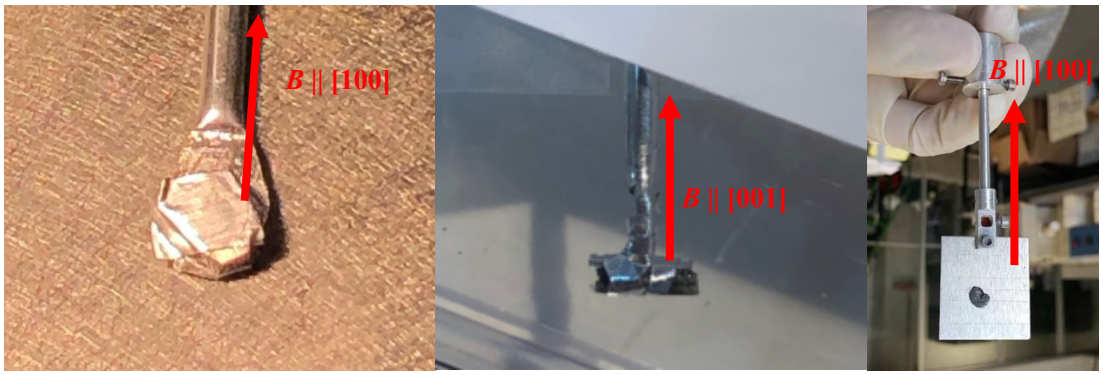

Figure S6. YMn_6Sn_6 single crystals used in our neutron scattering experiments. (a) Single crystal affixed to Al rod with small amount of super glue and wrapped in aluminum foil for in-plane magnetic field, [*H*, 0, *L*] scattering plane configuration at CORELLI. (b) Single crystal affixed to Al rod with small amount of super glue and wrapped in aluminum foil for *c*-axis magnetic field, [*H*, *K*, 0] scattering plane configuration at CORELLI. (c) Single crystal affixed to Al plate with CYTOP used in HB-3 triple axis experiment.

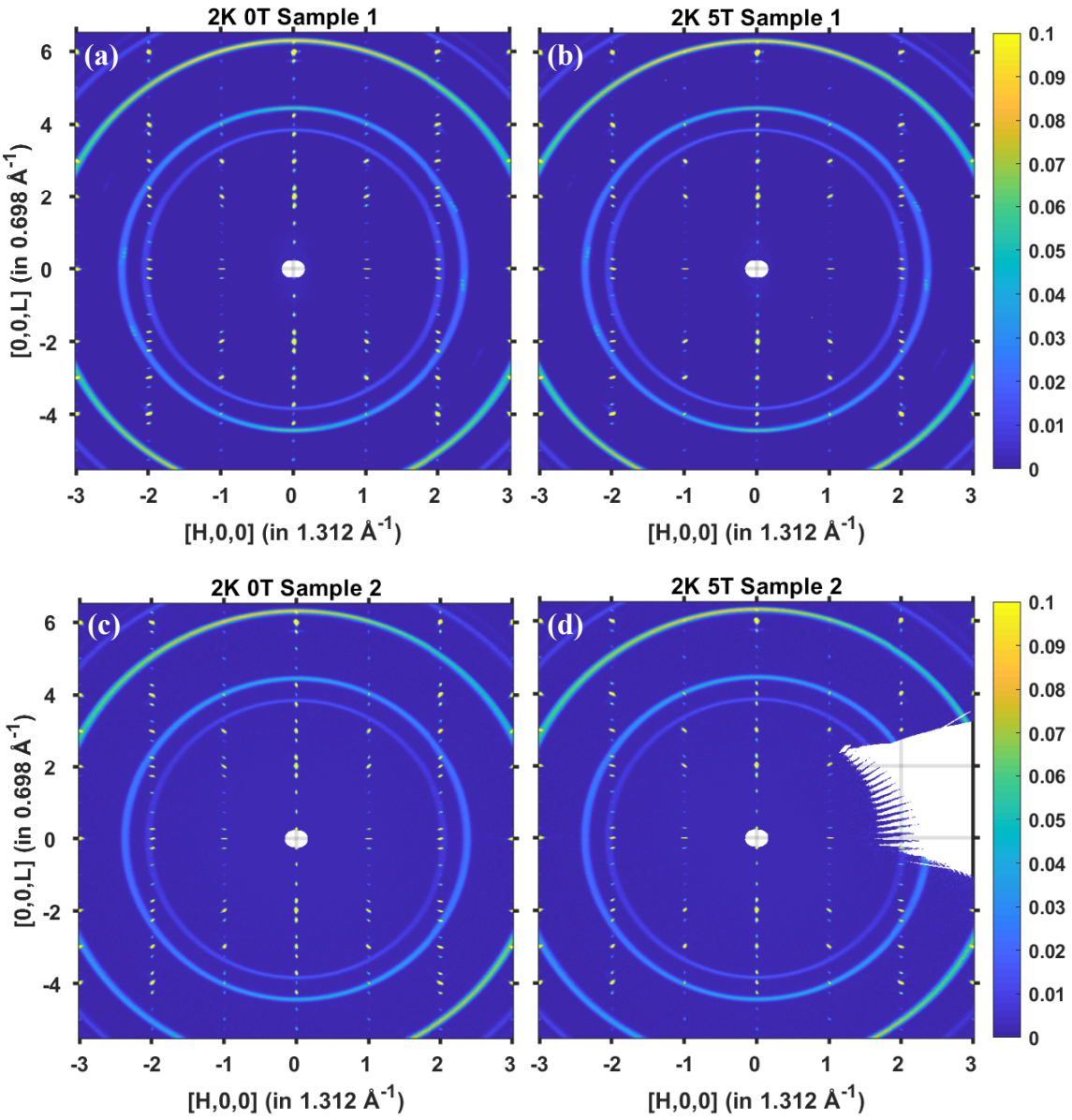

Figure S7. Raw data of the diffuse neutron scattering pattern of YMn_6Sn_6 at 2 K, (a) and (c) 0 T, (b) and (d) 5 T for samples 1 [(a) and (b)] and 2 [(c) and (d)] obtained on CORELLI. The data were collected by rotating the sample up to 360º along the vertical axis, with 1.5º apart between orientations.

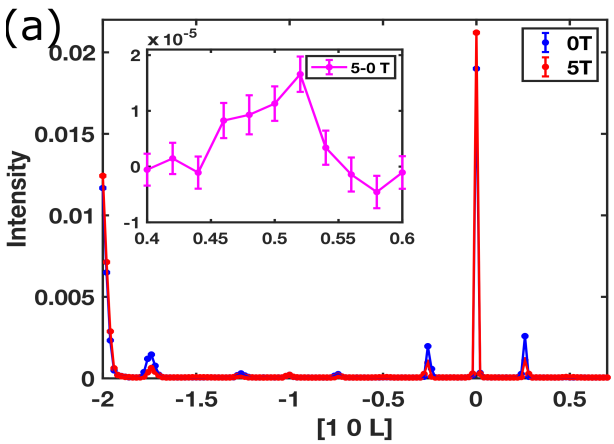

Figure S8. Magnetic field dependence of (a) [1, 0, *L*] at 2 K. Insets shows the (1, 0, 2δ) peak field off data subtracted from field on data.

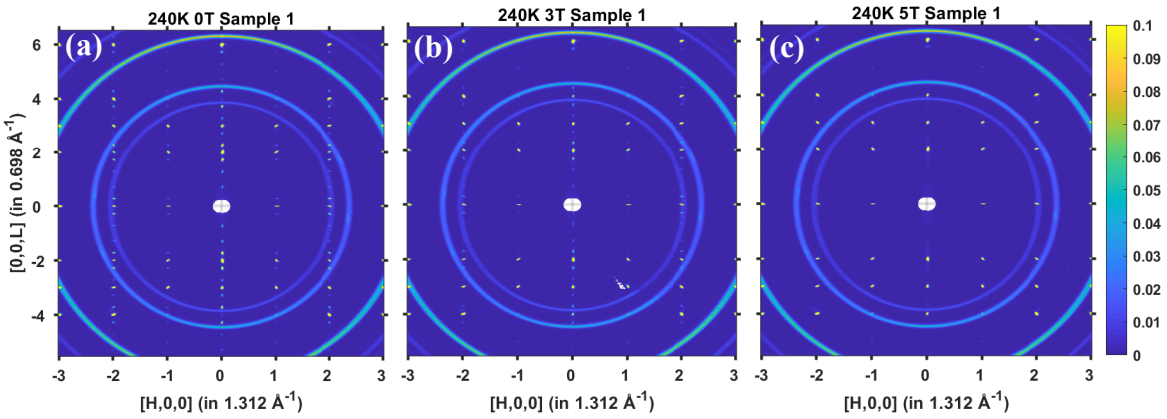

Figure S9. Raw data of diffuse neutron scattering pattern of YMn_6Sn_6 at 240 K, (a) 0 T, (b) 3T, and (c) 5 T obtained on CORELLI. The data were collected by rotating the sample 360º along the vertical axis, with 1.5º apart between orientations.

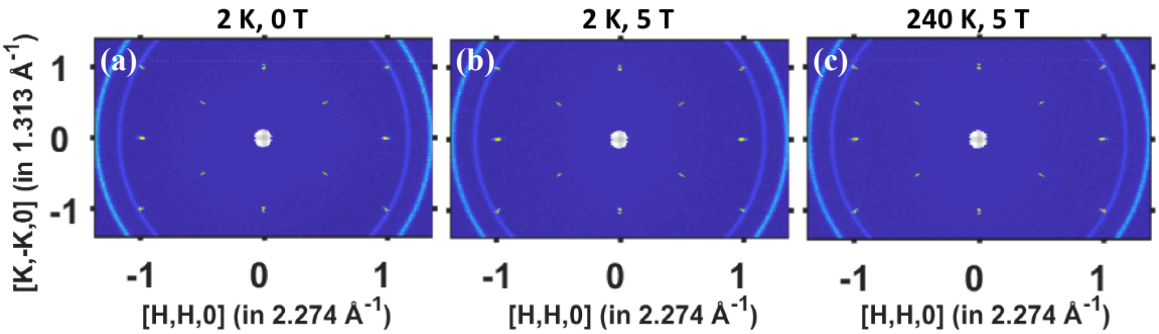

Figure S10. Raw data of diffuse neutron scattering pattern of YMn_6Sn_6 in the [*H*, *K*, 0] plane with field along the *c*-axis obtained on CORELLI at (a) 2 K, 0 T, (b) 2 K, 5 T, and (c) 240 K, 5 T.

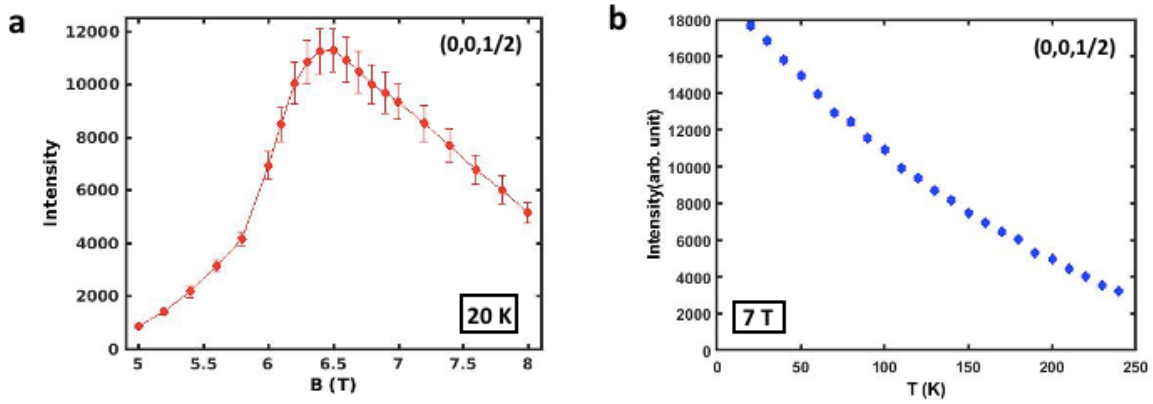

Figure S11. At 20 K, neutron diffraction measurements observe a new peak above 5 T at (0, 0, 0.5). (a) The (0, 0, 0.5) peak reaches a maximum intensity at ~ 6.5 T and is afterwards suppressed with increasing magnetic field. (b) When temperature is increased, under 7 T the (0, 0, 0.5) peak is suppressed until ~ 240 K. This corresponds to an unknown magnetic phase denoted "?" in the phase diagram [Fig. 3(a) of main text].

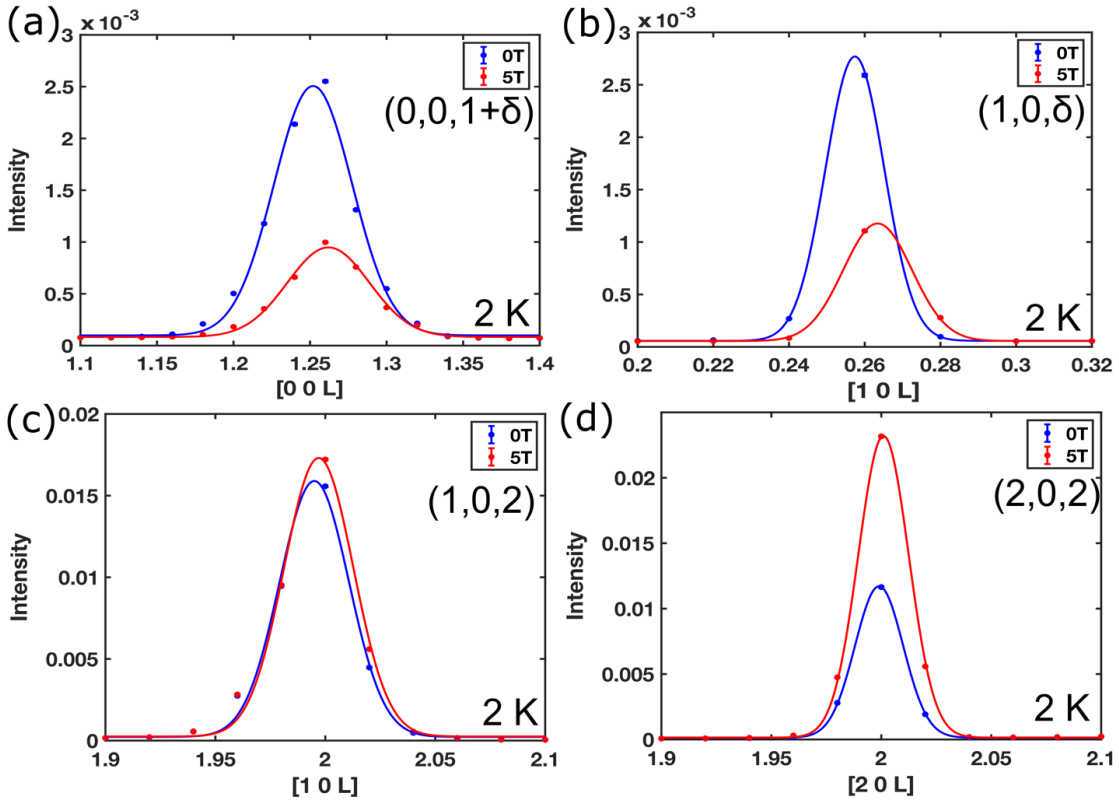

Figure S12. Magnetic field dependence of (a) the (0, 0, 1 + δ), (b) the (1, 0, δ), (c) the (1, 0, 2), and (d) (2, 0, 2) peaks at 2 K. Each peak is fit to a Gaussian.

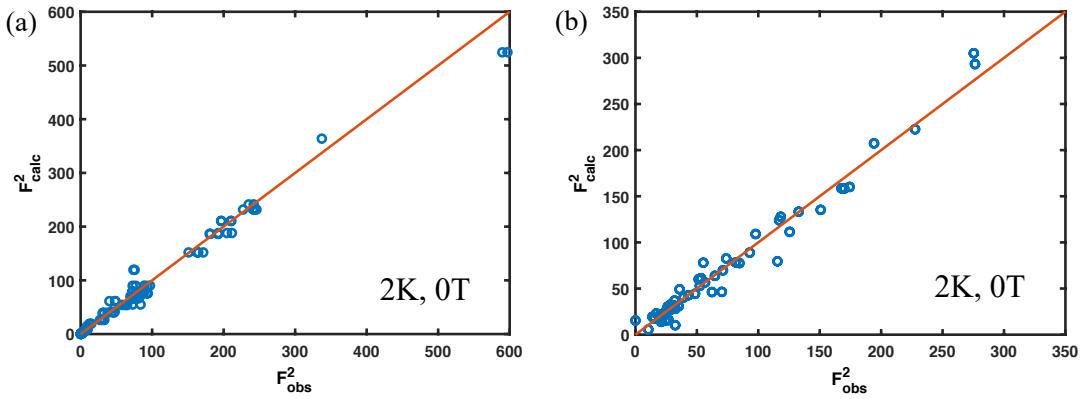

Figure S13. (a) The observed intensity plotted as a function of calculated intensity for the 2 K, 0 T nuclear refinement done using FullProf software. Red line is the $y = x$ guideline. The number of reflections used was 128 and the overall χ^2 = 14.8. (b) The observed intensity plotted as a function of calculated intensity for the 2 K, 0 T magnetic refinement done using Jana2006 software. Red line is the $y = x$ guideline. The number of reflections used was 125 and the overall χ^2 = 1.94.

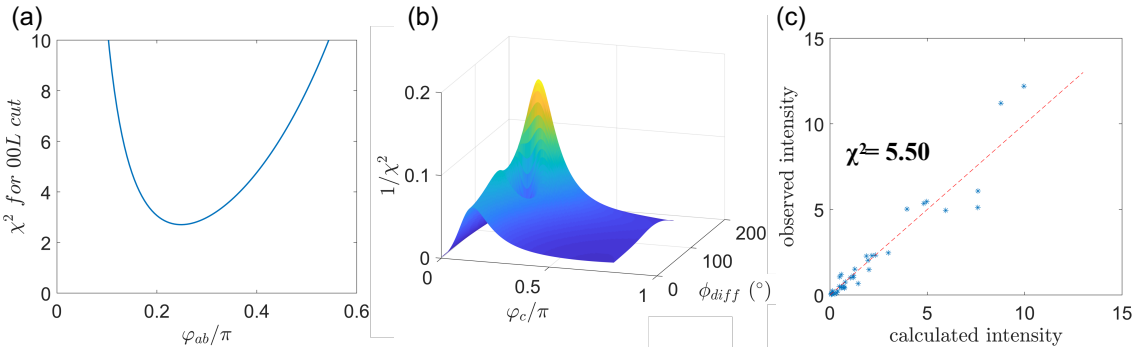

Figure S14. Fitting results for 2 K, 5 T data set. Shown in (a) is the χ^2 for (0, 0, L) cut fitting to determine ϕ_{ab}. The other two parameters, ϕ_c and φ is not relevant for the H = 0 dataset. Shown in (b) is the map of $1/\chi^2$ as a function of ϕ_c and φ while ϕ_{ab} is fixed at 0.24π. The optimal parameter set is ϕ_{ab} = 0.24π, ϕ_c = 0.265π, φ = 0.656π. Shown in (c) is the observed intensity plotted as a function of calculated intensity. Red dashed line is the $y = x$ guideline. Overall χ^2 = 5.5.

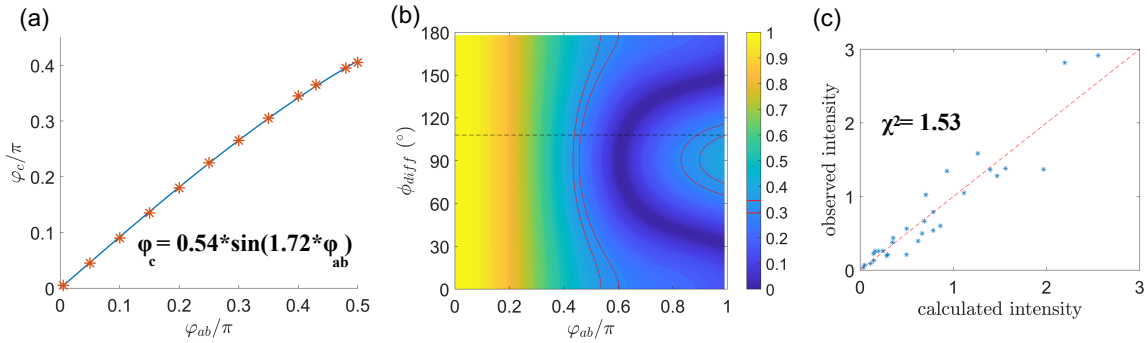

Figure S15. Fitting results for 240 K, 3 T dataset. Shown in (a) is the curve of optimal ϕ_c as a function of ϕ_{ab}. Shown in (b) is the contour map of total magnetization of the model as a function of ϕ_{ab} and φ, assuming ϕ_c follows the curve in (a). The magnetization measurement predicts the net moment at 240 K and 3 T to be within the red curves. The optimal parameter set is determined to be $\phi_{ab} = 0.455\pi$, $\phi_c = 0.38\pi$, $\varphi = 0.60\pi$. Shown in (c) the observed intensity plotted as a function of calculated intensity. Red dashed line is the $y = x$ guideline. Overall $\chi^2 = 1.53$.